1 **Characteristics of wintertime daily precipitation over the Australian Snowy Mountains**

2

3 **Fahimeh Sarmadi[a,b], Yi Huang[a,b], Steven T. Siems[a,b], Michael. J. Manton[a]**

4 [a]School of Earth, Atmosphere and Environment, Monash University, Victoria,

5 Australia [b]Australian Research Council (ARC) Centre of Excellence for Climate System

6 Science

7

8

9

10

11

13

14

15

16

17

18 Corresponding author address: Fahimeh Sarmadi, School Earth, Atmosphere and Environment,

19 Monash University, Victoria, Australia. Email: Fahimeh.sarmadi@monash.edu

20

21

22

23

24

25

26

Abstract

The relationship between orographic precipitation, low-level thermodynamic stability and the synoptic meteorology is explored for the Snowy Mountains of southeast Australia. A 21-year dataset (May-October, 1995-2015) of upper air soundings from an upwind site is used to define synoptic indicators and the low-level stability. A K-means clustering algorithm was employed to classify the daily meteorology into four synoptic classes. The initial classification, based only on six synoptic indicators, distinctly defines both the surface precipitation and the low-level stability by class. Consistent with theory, the wet classes are found to have weak low-level stability, and the dry classes have strong low-level stability. By including low-level stability as an additional input variable to clustering method, statistically significant correlations were found between the precipitation and the low-level stability within each of the four classes. An examination of the joint pdf reveals a highly non-linear relationship; heavy rain was associated with very weak low-level stability and, conversely, strong low-level stability was associated with very little precipitation. Building on these historical relationships, model output statistics (MOS) from a moderate resolution (12 km spatial resolution) operational forecast were used to develop stepwise regression models designed to improve the 24 hour forecast of precipitation over the Snowy Mountains. A single regression model for all days was found to reduce the RMSE by 7% and the bias by 75%. A class-based regression model was found to reduce the overall RMSE by 30% and the bias by 85%.

*Keywords***:** orographic precipitation, quantitative precipitation forecasts, model output statistics, 'Snowy Mountains'.

48

49

1. Introduction

The Snowy Mountains, with peaks in excess of 2000 m, are the tallest mountains in Australia and are part of a continental divide along the eastern seaboard, known as the Great Dividing Range. Precipitation to the west and north of these mountains naturally flows inland into the Murray and Murrumbidgee Rivers ultimately reaching the Great Australian Bight, while precipitation to the east naturally flows into the Snowy River reaching the Tasman Sea (Figure 1a). This water is of immediate economic value for the generation of hydroelectric power and is of further value for downstream consumption, particularly for agriculture across the semi-arid Murray-Darling Basin. For this reason, water is routinely diverted through a series of tunnels, aqueducts, and pumps from the Snowy River Basin across the divide into the inland catchments. The day-to-day management of this water resource requires accurate quantitative precipitation estimates and forecasts over the mountains.

Distinct from daily forecasts and estimates, the climatology of precipitation has been of great interest, particularly over the last decade. For instance, Landvogt et al. (2008) produced a climatology of wintertime precipitation in the Australian Alpine regions, in which daily precipitation was categorized into synoptic clusters consisting of "pre-frontal", "post-frontal", and "cutoff" classes. Chubb et al. (2011) studied a 20-year period from 1990, which included most of the 'millennium drought', one of the most severe droughts in the past century (Timbal 2009). Through this period, a 43% decline in wintertime precipitation at high elevations (greater than 1000 m) was observed. Local weather systems were classified into three major synoptic types (embedded lows, cutoff lows and other) based on the synoptic mean sea level pressure (MSLP) and the 500-hPa geopotential height. Dai et al. (2014; D14 hereafter) assigned the daily synoptic meteorology into one of four classes using a K-means clustering algorithm with the upwind upper-air sounding. They found that the two wet clusters accounted for 30%

75 of all days and 70% of the total wintertime precipitation. These two wet classes were associated

76 with fronts (both embedded and cutoff) and post-frontal conditions, respectively. Fiddes et al.

77 (2015) employed a set of circulation dynamics indices to show that there has been a continuing

78 decline in western-high-elevation winter time precipitation of alpine Australian and a relatively

79 stable rainfall trend in eastern parts of this region. These distinct phenomena are hypothesized

80 to be caused by the likely presence of complex relationships between the amount of

81 precipitation and large-scale climate patterns over this region, especially for extreme events

82 (Theobald et al. 2015).

83   Orographic precipitation is commonly defined as precipitation arising from the lifting of

84 moist air in response to the presence of the mountains. Fundamentally, orographic precipitation

85 depends on the local upwind lower atmospheric stability, commonly referred to as the non-

86 dimensional mountain height $\hat{H}$, or the inverse Froude number (Pierrehumbert and Wyman

87 1985). Smith (1989) developed a regime diagram for hydrostatic flow over a mountain to

88 illustrate the stagnation onset as a function of the spanwise-to-streamwise horizontal aspect

89 ratio of the topography and $\hat{H}$. Orographic precipitation is also known to be sensitive to small

90 variations in ambient conditions, the evolution of the moisture fields, and the geometry of the

91 barrier (e.g. Colle 2004; Watson and Lane 2012). These variations give rise to a variety of

92 distinct dynamical and microphysical mechanisms that are classified as orographic

93 mechanisms (Houze 2012).

94   Forecasting orographic precipitation with a numerical weather predication (NWP) model

95 is challenging due not only to the difficulties of representing the variety of complex physical

96 mechanisms, but also to the limited resolution of a simulation to resolve the complex surface

97 geometry (e.g. Panziera 2010). The evaluation of precipitation forecasts is a further challenge

98 given the high spatial variability of precipitation across a complex terrain, and the limited

99 number of surface sites available that can be used to rigorously evaluate the simulations.

Another challenge for local forecasts lies in the unique environment of the Snowy Mountains, which distinguishes itself from other mountainous regions of the world (e.g. the Sierra Nevada in the western US) by the frequent presence of clouds comprised of supercooled liquid water (SLW, Morrison et al. 2013). The development of precipitation in mixed-phase clouds remains poorly understood and difficult to model (e.g. Furtado et al. 2016). Osburn et al. (2016) reported a high frequency of occurrence of SLW (53% of the time between April and September) over the Snowy Mountains from a surface-based radiometer located on the upwind slope. These observations were qualitatively consistent with those from the MODerate-resolution Imaging Spectroradiometer (MODIS) satellite product. As a further challenge, Chubb et al. (2015) found a high catch-ratio loss in the winter precipitation over the high elevation sites in the Snowy Mountains due to the lack of heated tipping-bucket gauges and wind fences.

Given the many challenges in numerically simulating orographic precipitation, a common practice has been to develop statistically based models to forecast precipitation as a function of some independent predictors (i.e. a regression between synoptic and/or local indicators to forecast precipitation). Statistical models are relatively simpler than NWP models; however, they do not consider the various physical processes of precipitation. Therefore, a combination of current NWP and statistical models seems to be an appropriate solution to address the above-mentioned limitations. Model Output Statistics (MOS) is a commonly used, post-processing technique to improve the skill of NWP forecasts, employing a statistical method to relate model output to observations (Glahn and Lowry 1972). Examining an ensemble NWP precipitation forecast, D14 found a significant underestimation of precipitation intensity over the high elevation terrain of the Snowy Mountains. Using their synoptic clustering, they applied a linear regression algorithm to improve the performance of ensemble precipitation forecasts, reducing the root mean square error (RMSE) by over 20% for their two wet clusters. The ensemble

125   model, known as the Poor Man's Ensemble (Ebert et al. 2001), combined the output of seven

126   independent large-scale NWP models to forecast precipitation at a coarse spatial scale of 1° ×

127   1° resolution.

128   One of the broader aims of the current research is to evaluate the performance of the high-

129   resolution Australian Community Climate and Earth-System Simulator (ACCESS) NWP

130   system (Puri et al, 2013) in forecasting wintertime precipitation across the high elevation

131   terrain of the Snowy Mountains. A further aim is to test whether the method developed in D14

132   (based on building a statistical relationship between the variables from synoptic classification

133   and the ensemble forecast of rain to enhance the skill of the model in precipitation intensity

134   prediction) is applicable to an operational, high-resolution precipitation forecasts provided by

135   the ACCESS model. Finally, we seek to improve this clustering based MOS methodology by

136   extending the analysis to explicitly consider the lower atmosphere stability. Limiting our

137   analysis to the cold seasons (May – October), the main outcomes of this study are: i) the

138   categorization of the low-level atmospheric stability, $\hat{H}$, for the Snowy Mountains, ii) the

139   investigation of inter-dependences between the low-level atmospheric stability and the daily

140   precipitation, and iii) the improvement in the accuracy of the daily NWP precipitation forecasts

141   over the Snowy Mountains via stepwise regressions coupled with the results of synoptic

142   categorization.

143

144   **2. Datasets**

145   **2.1. Ground-based wintertime precipitation dataset**

146   Half-hourly precipitation is obtained from seven weather stations above 1100 m across the

147   Snowy Mountains for a 21-year period from 1995 to 2015. These high-elevation gauges,

148   operated by Snowy Hydro Ltd. (SHL), utilize well-maintained heated tipping buckets for

149   precipitation measurements. For consistency with the sounding, daily precipitation is obtained

150 by aggregating the half-hourly precipitation from 10:00 local time (00 UTC) to the same time

151 of the next day. Chubb et al. (2011 and 2016) have evaluated the quality of the precipitation

152 gauge data, finding appropriate accuracy and reliability of these measurements for

153 climatological studies. The locations of the gauges and their long-term mean wintertime

154 precipitation (May-October) are shown in Figure 1b and Table 1, respectively. For the 21-year

155 period considered, a full daily record (no missing data) of all stations was available for

156 approximately 60% of the time. When data from one or more sites was either completely

157 missing or its quality was flagged, the area-average daily precipitation was taken to be the mean

158 of the remaining valid observations. No systematic bias in missing or flagged data has

159 previously been noted. For the winter period 2014-2015, 92% of all days have at least five

160 stations that had valid data contributing to the mean value.

161

162 **2.2. ACCESS model dataset**

163 The model data examined in this study are taken from the current operational ACCESS

164 NWP system. The atmospheric component of ACCESS is the UK Met Office Unified Model

165 (MetUM), which is a non-hydrostatic model using a semi-implicit, semi-Lagrangian numerical

166 scheme (Davies et al. 2005) to solve deep-atmosphere dynamics. This version of the ACCESS

167 NWP system is referred to as the "Australian Parallel Suite 1" (APS1), which represents the

168 first major upgrade to the system since operational running commenced in August 2010. The

169 ACCESS-R forecasts used in our study for the two year (2014-2015) cold months (May-

170 October) is the Australian-wide regional domain model that covers an area of 65°S-16.95°N

171 and 65°E-184.57°E. This model has a horizontal resolution of ~12km (0.11°) and a vertical

172 resolution of 50 levels with the highest level at 37.5 km. Benefiting from the 4-D data

173 assimilation, the ACCESS-R forecasts are initialized at 0000, 0600, 1200 and 1800 UTC of

174 each day and provides hourly precipitation forecasts up to 72 hours ahead. The forecast

175 precipitation is the sum of two components that are computed separately in the model using

176 the convective and large-scale (i.e. microphysics) parameterization schemes, respectively.

177 More detailed information on the ACCESS-R can be found in Puri et al. (2013). For this study,

178 the mean value of 10 grid boxes covering the Snowy rain gauges, bounded by latitudes 35.85°-

179 36.40°S and longitudes 148.27°-148.49°E, is employed to represent the ACCESS-R

180 precipitation forecast over the high elevations of Snowy.

181

182 **2.3. Wagga Wagga sounding dataset**

183 The nearest upwind sounding site to the Snowy Mountains is at Wagga Wagga, located

184 about 180 km to the northwest (Figure 1a). Both Chubb et al. (2011) and D14 successfully

185 employed these soundings to define the synoptic meteorology during the cold seasons. For the

186 winter period of 1995-2015, the 00 UTC sounding data were obtained from the database of

187 University of Wyoming (http://weather.uwyo.edu/upperair/sounding.html). Soundings were

188 available for 75% of the days (2897 out of 3843).

189 Following D14, as a first step we employ a cluster analysis with six synoptic indicators

190 calculated from the Wagga Wagga soundings to investigate interactions between the large-

191 scale environment and daily winter precipitation across the Snowy Mountains. The synoptic

192 indicators chosen are: i) surface pressure at Wagga Wagga (GP), ii) southerly moisture flux up

193 to 250 hPa (QV), iii) westerly moisture flux up to 250 hPa (QU), iv) total moisture up to 250

194 hPa (TW), v) root-mean-square wind shear between 850 and 500 hPa (SH), and vi) total totals

195 index (TT). More details regarding these indicators can be found in Table 2. Briefly, the three

196 indicators TW, QV and QU represent the available amount of water for the formation of

197 precipitation, while TT and SH are considered to be simple estimates of the static stability of

198 the atmosphere (Henry 2000).

199   Expanding on the framework of D14, the low-level atmospheric stability, i.e. the non-

200   dimensional mountain height ($\hat{H}$), is added as a seventh predictor. TT and SH are defined

201   between the levels of 850 and 500 hPa; whereas $\hat{H}^2$ is defined to a height of 1000 m. The

202   mathematical expression of the non-dimensional mountain height is

$$\hat{H} = \frac{1}{Fr} = \frac{Nh}{U} ,\tag{1}$$

204   where U is the cross-mountain wind speed (m/s) and h is the mountain height (h=1 km

205   representing the mean elevation of the region (e.g. Reinecke and Durran 2008). N is the Brunt-

206   Vaisala frequency (s^{-1}). Following Hughes et al. (2009), the moist Brunt-Vaisala frequency

207   (Durran and Klemp 1982) is employed when the relative humidity is greater than 90% (i.e.

208   saturated conditions), otherwise the dry Brunt-Vaisala frequency is adopted. As the value of N

209   is imaginary when the atmosphere is conditionally unstable, so is the value of $\hat{H}$. In order to

210   account for conditionally unstable events, which occur about 11% of the time, we employ the

211   square of the $\hat{H}$ values ($\hat{H}^2$) for all analysis. Negative values of $\hat{H}^2$ indicate conditional

212   instability. Hughes et al. (2009) showed that the large square Froude number values have

213   similar behaviour as the negative ones (known also as conditionally unstable).

214   For small $\hat{H}^2$ values, the low-level atmospheric conditions are generally referred to as being

215   unstable to orographic lifting, implying that the airflow can readily pass over the terrain and

216   mountain waves will be generated. For large $\hat{H}^2$ values, the flow can be stagnated or diverted

217   laterally around the barrier instead of being lifted over the terrain. In this scenario, stable or

218   blocked conditions (hereafter "blocked days") are generally observed (e.g. Watson and Lane

219   2014; Miao and Geerts 2013; Wang et al. 2016). Following the literature, we use $\hat{H}^2$ equal to

220   1 as the threshold to distinguish stable and unstable conditions. In practice, however, the

221   transition is not precise, especially as we use only a fixed estimate for the mountain height, h.

222   As discussed, the spatial distribution, magnitude and frequency of orographic precipitation has

223 commonly been found to be sensitive to $\hat{H}^2$. When $\hat{H}^2 < 1$ (unblocked days here), heavier

224 precipitation events can be expected (e.g. Miglietta and Buzzi 2001; Colle 2004; Wang et al

225 2016). By inspecting the coastal winds of California, Hughes et al. (2009) showed that the

226 spatial distribution of precipitation became more homogenous for blocked cases, while for

227 unblocked flows local orographic precipitation was strongly dependent on the slope of

228 topography.

229

230 **2.4. ERA-Interim reanalysis dataset**

231 Following Theobald et al. (2015), we employ the ERA-Interim reanalysis products (Dee et

232 al. 2011) provided by the European Centre for Medium-Range Weather Forecasts (ECMWF)

233 to derive composite synoptic charts that correspond to the clusters. The ERA-Interim data we

234 employ are from 1995 onwards and at a spatial resolution of $0.75° \times 0.75°$. As the soundings

235 at Wagga Wagga were not available at all time, the six synoptic indicators and $\hat{H}^2$ obtained

236 from the ERA-Interim reanalysis dataset are used to fill in missing physical soundings for days

237 in 2014-15. Comparisons of the in-situ Wagga Wagga soundings and the corresponding ERA-

238 Interim reanalysis soundings for common days over the 21-year winter period show strong

239 correlations for all synoptic indicators (GP: 0.99, SH: 0.90, TT: 0.92, TW: 0.97, Qv: 0.98, Qu:

240 0.97). Therefore, we consider using the ERA-Interim reanalysis soundings as a surrogate is

241 appropriate. We note that as the Wagga Wagga soundings are likely employed in the data

242 assimilation for ERA-Interim, the two sets of soundings may not be completely independent.

243 The ERA-Interim soundings may be less skilled when the physical soundings are not available.

244

245 **3. Methodology**

246 **3.1.Cluster analysis**

247   The weather systems in southeastern Australia can be classified using simple clustering

248 methodologies such as *K*-means (Hartigan and Wong 1979). Recent studies by Wilson et al.

249 (2013) and D14 show that winter days in Australia can be categorized into unique synoptic

250 regimes by utilizing six synoptic indicators as independent variables for the clustering

251 procedure, applied in the present study as well. In addition to these six indicators, $\hat{H}^2$ is also

252 employed to account for the low-level local atmospheric stability.

253   Determining the optimal number of clusters using the *K*-means algorithm is challenging

254 given the opposite relationship between the number of clusters and their variances. Following

255 D14, the optimal number of clusters is determined when the probability distributions of the

256 daily rainfall for different clusters can be separated distinctively. Given that a relationship

257 between orographic precipitation and $\hat{H}^2$ is expected (Colle 2004), it is also worthwhile to

258 appreciate the probability distributions of $\hat{H}^2$ for each cluster when only the original six

259 indicators are employed for the cluster analysis. A two-sample Kolmogorov-Smirnov (KS) test

260 is applied to insure the distinctiveness of the distributions.

261

262   **3.2. Model Output Statistics approach in precipitation forecasting**

263   The main aim is to improve the daily ACCESS-R precipitation forecasts (Prec_Acc) by

264 combining the results of the synoptic classification with a stepwise regression. To this end, the

265 averaged high-elevations SHL rain gauge observations are taken as the "ground truth" for this

266 analysis. As the aim is to develop an operational MOS algorithm, the six predictors and $\hat{H}^2$ are

267 taken from ACCESS-R instead of the physical soundings. Note that, due to operational

268 management issues, the number of daily soundings at the Wagga Wagga station has been

269 reduced to roughly three per week (i.e. available 154 days during two-winter period of interest)

270 in recent years.

271   To assess the skill of ACCESS-R in representing the synoptic regimes as observed by the

272   physical soundings, the six synoptic indicators derived from the Wagga Wagga and ACCESS-

273   R soundings are compared for the same time window (2014-15). The pairwise Pearson

274   correlations between synoptic indicators showed significant correlations (at the level of 0.05)

275   ranging from 66% (for SH) to 99% (for GP), suggesting a good agreement between the model

276   and the observations. Based on this, the synoptic classification scheme is applied to the

277   ACCESS_R soundings. The results show high consistency, justifying the use of the synoptic

278   classification on the ACCESS-R soundings for deriving the regression equations.

279   As discussed above, within a forecasting context, all variables are taken from the

280   ACCESS_R outputs, including the definition of a rain day. Model 1 is a single regression for

281   all 366 winter days, regardless of cluster. Model 2 first classifies each day into one of the four

282   clusters, with each cluster having its own regression.

283   The seven predictors and the ACCESS-R precipitation data were normalized before the

284   regression models were developed. Model selection/complexity is an obvious problem when a

285   large number of predictors are available. A stepwise approach (from a single constant value to

286   quadratic combinations, including an intercept, linear terms, products, and squared terms) was

287   applied to determine the leading predictors and the optimum regression formulation (degree of

288   complexity within equations). Measures of accuracy (e.g. the RMSE or bias) will automatically

289   improve as more predictors are included, but this comes at the cost of model simplicity. To

290   balance the complexity and accuracy, the number of predictors employed was determined by

291   minimizing the Bayesian Information Criterion, BIC, as an objective function (Liebscher 2012).

292   The BIC is expressed as:

$$BIC = k \cdot \ln(n) - 2 \cdot \ln(\hat{L}) \qquad (2)$$

294   where k is the number of free parameters to be estimated, n is the number of observations and

295     $\hat{L}$ is the maximized value of the likelihood function of the model. Further, we have considered

296 a stepwise procedure that entails a forward selection and backward elimination algorithm. This

297 process includes an examination of any linear dependency between predictors (called as

298 multicollinearity) with redundant variables removed regardless of the goodness-of-fit criterion

299 value (Curtis and Ghosh 2011).

300 Both regression models were cross-validated via a bootstrapping methodology with 10000

301 simulations to ensure that the results were statistically robust. For each simulation, 80% of the

302 data are randomly assigned to the control group (used for deriving the coefficients) and the rest

303 for testing.

304

305 **4. Results**

306 **4.1. Winter precipitation characteristics**

307 Following Chubb et al. (2011), a rainy day is defined at a threshold of 0.25 mm day^{-1} for

308 either the average SHL surface observations or ACCESS-R precipitation. A basic summary of

309 the winter precipitation is provided in Table 3. The frequency of rainy days is seen to follow a

310 seasonal cycle with peaks being present in July and August. The intensity, however, is not

311 found to present such a cycle; an overall mean intensity of 10.4 mm day^{-1} is observed for rainy

312 days, with a standard deviation of 13 mm day^{-1}. The mean intensity can be broken down into

313 quartiles, which again do not display any strong seasonal cycle over the course of winter.

314 Average monthly precipitation on rain days indicates lower values in the transition months of

315 May and October with an overall wintertime mean precipitation of about 167 mm.

316 Focussing on the two-year analysis period (2014-2015), the SHL surface observations

317 show a reduction in both the frequency of rainy days and the intensity (not significant at the 5%

318 level) compared to the climatology. The statistics with ACCESS-R, show that both the

319 frequency and intensity are greater than the observed values (not significant at the 5% level).

320

4.2. Synoptic classification

The K-means clustering technique was applied to the Wagga Wagga soundings data

(complemented with ERA-I soundings for days when the physical soundings were unavailable)

for winter days for the 21-year period 1995-2015 using the six indicators. When employing the

original six sounding variables (TT, SH, QU, QV, GP & TW), the new analysis was consistent

with that of D14; four clusters were the maximum number found to produce distinct daily

rainfall probability distributions (Figure 2, left panel), passing the KS test at the 5%

significance level. As a major objective of this research is to better understand the nature of the

low-level stability, $\hat{H}^2$, over the Snowy Mountains, and its value as a predictor of orographic

precipitation, daily $\hat{H}^2$ probability distributions are also produced (Figure 2, right panel). As

with the daily precipitation, four clusters lead to distinct distributions of $\hat{H}^2$, suggesting that

the low-level stability is reflected in the broader synoptic meteorology.

A K-means clustering was then undertaken using the original six synoptic variables and $\hat{H}^2$

(7-variable clustering results are only elaborated hereinafter). As before, four clusters were

found to be necessary to distinctly represent the daily precipitation distribution (not shown).

C1 and C2 were found to be quite stable to this revision with only a handful of days swapping

between clusters. The two dry clusters, however, were found to be more sensitive to this

clustering revision. 1037 out of the original 1123 days in C3 remain unchanged (5 days shifted

to C1, 50 days to C2, and 31 days to C4), while 823 of the original 1003 days in C4 remain

unchanged (35 days shifted to C2, and 145 days to C3). This further suggests that for the wet

clusters, C1 and C2, that the low-level stability is reflected in the synoptic meteorology.

According to Table 4, clusters C1 (frequency of rainy days: 93%, median: 18 mm day^{-1}) and

C2 (frequency of rainy days: 78%, median: 4.54 mm day^{-1}) represent the wettest groups while

C3 (frequency of rainy days: 52%, median: 0.32 mm day^{-1}) and C4 (frequency of rainy days:

22%, median: 0.03 mm day^{-1}) capture the driest weather. There are fewer days of C1 and C2

346 than C3 and C4. The mean values of $\widehat{H}^2$ for the four clusters are -0.45, 1.97, 6.24 and 20.20,

347 respectively. Higher values of $\widehat{H}^2$ indicate stronger blocking and, accordingly, less orographic

348 precipitation. The fraction of unblocked days ($\widehat{H}^2 < 1$) for the four clusters are 63%, 48%, 20%

349 and 5%, respectively. The probability density functions (PDF) of $\widehat{H}^2$ are broken down by

350 cluster (Figure 3, a-d) for all days. Distribution of $\widehat{H}^2$ for all days is shown in stacked

351 histogram in Figure 3e. For rainy days only, the PDF will be shifted to lower (less stable) values

352 of $\widehat{H}^2$, and for no rain days shifted to higher ones (more stable) (Figure 3f). The seasonal

353 variability of clusters is also found to be consistent with D14, the relative frequencies of C1

354 and C2 increase towards the end of winter. C3 is more frequent in early winter and C4 occurs

355 more often in midwinter (not shown). Further, the synoptic meteorology of the wettest cluster

356 C1, is consistent with the analysis of Chubb et al. (2011), a strong northwesterly moisture flux

357 and low surface pressure are commonly present.

358   To better appreciate the synoptic meteorology of these four clusters (based on 7-variable

359 clustering), ERA-Interim data are used to construct composite maps of the large-scale synoptic

360 indicators for each cluster (Figures 4-6). Following Theobald et al. (2015), the map domain is

361 20- 46°S and 120°-140°E in order to capture the dominant synoptic meteorology. For these

362 maps, only the top 25% of days of each cluster are employed. Specifically, these are the days

363 that have the shortest Euclidean distance to the cluster centre. While this approach is commonly

364 used when employing daily observations (e.g. Pook et al. 2006, Theobald et al. 2015), it has

365 been noted that the daily resolution of composite maps may mask some unresolved features

366 within daily systems (e.g. a diurnal cycle), as well as over-represent slow-moving synoptic

367 systems (Gallant et al. 2012).

368   Starting first with the MSLP and total water (Figure 4), general synoptic states can be

369 assigned to the four clusters. The MSLP for C1, suggests that the cluster is associated with a

370 frontal passage. It is not possible to distinguish between a cut-off low and an embedded low

14

due to the compositing technique and the low number of clusters. Further, C1 is associated with a maximum in total water over the mountains, which is seen to extend up the Great Dividing Range through New South Wales and Queensland. Chubb et al. (2011) employed a back-trajectory analysis to define a 'moisture corridor' across this region for heavy precipitation events. C2, while less well resolved, suggests that the frontal system has passed over mountains. Chubb et al. (2012) detailed a case study of a frontal passage over the nearby Brindabella ranges, where orographic precipitation was recorded over the 24-hour period after the passage of a front. Here air originating from the Southern Ocean brings limited moisture and modest precipitation. Skipping to the dry cluster C4, a strong high pressure system is evident over the region with very little moisture available. Cluster C3 is less easy to classify, most likely including a variety of synoptic settings that ultimately lead to little precipitation. A high-pressure ridge is present across central Australia in the composite map, although it is much weaker than that of C4.

Turning to the moisture fluxes (Figure 5), the strong northerly and westerly moisture fluxes of C1 stand out, consistent with a frontal passage. There is virtually no northerly moisture flux over the Snowy Mountains for C2. It is strictly a westerly flux that is bringing the moisture for precipitation, again suggesting a post-frontal environment (Chubb et al. 2012). Spatially, C3 and C4 are quite similar, with weak fluxes evident over the mountains. C4 is drier and has weaker fluxes of the two.

The synoptic stability composites (TT and SH, Figure 6) further complete the general classifications of clusters C1 (frontal), C2 (post-frontal) and C4 (high pressure system). Over the mountains, the atmosphere is most unstable during a frontal passage and most stable under a high-pressure system. Unlike the other composite maps, however, these maps for C3 are now quite distinct, especially for the mid-level shear (SH). Very weak shear is evident just to the south of the Snowy Mountains, over Bass Straight and extending into the Tasman Sea. This

396 perhaps suggests that the upper free troposphere may be important in defining the synoptic

397 meteorology of this cluster. A more thorough analysis of C3 revealed that a number of the days

398 included in the composite included 'east coast lows' (BoM 2017) (e.g. 02 Oct. 2004 and 18

399 Sept. 2015).

400 A number of studies have diagnosed the principal synoptic types in southeastern Australia (e.g.

401 Chubb et al. 2011; Pook et al. 2006). Specifically, Theobald et al. (2015) applied an automated

402 approach to generate synoptic types by combining meteorological variables throughout the

403 depth of the troposphere across the Snowy Mountains. It is interesting to compare and contrast

404 our four wintertime clusters with their 11 synoptic types. Only a limited comparison is possible

405 as Theobald et al. (2015) considered only heavy precipitation days (threshold of 10 mm day^{-1})

406 for the full year. Further, instead of employing physical observations from a sounding site,

407 they employed 13 variables provided from the ERA-Interim reanalysis. In spite of these

408 substantial differences, it is evident from the composite maps that C1 and C2 correspond to

409 Theobald clusters T5 (Prefrontal troughs; approaching cold fronts) and T1 (Embedded cold

410 fronts). Not surprisingly, dry clusters C3 and C4 (occurring ~70% of the time during the cold

411 seasons and most frequently at the start and middle of winter) were not represented by any of

412 the Theobald clusters, since their analysis was limited to wet conditions throughout the year.

413 In summary, C1 includes the heaviest precipitation days and the lowest $\hat{H}^2$ values (and the

414 highest frequency of unblocked cases). It occurs for 10% of the winter days, but accounts for

415 39% of the precipitation. It is associated with frontal passages. C2 is associated with post-

416 frontal conditions. It occurs 22% of the time and accounts for 33% of the precipitation. C3 is

417 associated with a variety of synoptic conditions. It is a dry cluster, occurring 40% of the time

418 and accounts for 23% of the total precipitation. Finally, C4 is the driest cluster associated with

419 high-pressure system dominating the region over the Snowy Mountains and to its north. This

420   occurs ~30% of the time and accounts for only 5% of the precipitation. It has also the strongest

421   low level stability (i.e. highest $\hat{H}^2$ values).

422

423   **4.3. Relationships between independent variables and observed precipitation**

424   Given that an aim of this research is to improve orographic forecasts of precipitation

425   through model output statistics, it is worthwhile to examine the correlation of these predictors

426   with the precipitation. Working with the historic data (1995-2015), QV (-0.51), QU (0.46), GP

427   (0.46) and TW (0.43) are highly correlated with precipitation, while the stability measures $\hat{H}^2$

428   (-0.24), TT (0.23) and SH (0.16) are less strongly correlated. All correlations are statistically

429   significant, confirming our underlying premise that these variables can be of use in forecasting

430   orographic precipitation. Table 5 also illustrates the cross-correlations between these variables

431   at the 0.01 significant level. The highest significant correlation is between GP-QU (-0.53);

432   while, the lowest significance is for SH-TT (-0.136). SH-TW and SH-QV did not indicate

433   significant linear correlations.

434   Returning to the correlation between precipitation and the seven predictors, it is worthwhile

435   to break down the analysis to the four clusters (Table 6). Not surprisingly, the correlation

436   between the precipitation and any predictor is reduced within an individual cluster defined by

437   these predictors. While greatly reduced, the correlations of QV, QU, GP, and $\hat{H}^2$ remain

438   statistically significant within each of the four clusters. TW remains significantly correlated

439   within C1, C2 and C3. SH is only significantly correlated with precipitation in C4. Table 6 also

440   details the rank correlation of these predictors against the precipitation. For the three stability

441   predictors (SH, TT, and $\hat{H}^2$), the rank correlation (measures the degree of similarity between

442   two rankings assigned to two members of a set) is greater in magnitude than the linear

443   correlation suggesting a non-linear relationship exists between precipitation and stability. The

444   rank correlation for $\widehat{H}^2$ is nearly as great in magnitude as that for GP, both of which are

445   negative.

446   To better appreciate the inter-dependencies between $\widehat{H}^2$ and precipitation, their joint

447   probabilities are explored with the use of a copula function (Sklar 1959). Copula functions have

448   been widely used (e.g. Drouet-Mari and Kotz 2001, Genest and Plante 2003, Nicoloutsopoulos

449   2005) to detect the probabilistic relationships between variables and to show that a set of

450   variables with low correlations (even zero) may still retain complicated "tail" dependence

451   structures. Unlike the commonly used correlation measures, copulas are invariant under strictly

452   increasing transformations of random variables which are used for comprehensively exploring

453   nonparametric measures of interdependence (Schweizer and Wolff 1981). Copulas are not

454   restricted to any particular type of parametric functions (e.g. Gumbel distribution) for the

455   marginal or the joint probability distributions (Madadgar and Moradkhani 2014). According to

456   Figure 7A, the scatter plot and marginal histograms illustrates the relationship between

457   precipitation and $\widehat{H}^2$ in which, in overall, large values of precipitation are associated with low

458   values of $\widehat{H}^2$ and high values of $\widehat{H}^2$ are associated with weak precipitation. The marginal

459   histograms further indicate that the vast majority of data are located in the range of 0.25 mm

460   to 10 mm for precipitation and -1 to 5 for $\widehat{H}^2$, overwhelming the "tail" observations outside

461   this range.

462   Figure 7B and 7C illustrate the marginal CDF distributions of $\widehat{H}^2$ (ranging from -5 to 25)

463   and precipitation (ranging from 0 up to 100 mm) for rainy days based on the data from 1995-

464   2015. A steep slope implies a higher density of data within a considered range; precipitation

465   values less than 10 mm and $-1<\widehat{H}^2<5$ have the highest frequency of occurrences (similar to

466   what is concluded from the marginal histograms). Figure 7B and 7C are the main input

467   elements used in calculating the joint probability values and forming copula function. The

468   Frank copula (Frank 1979), selected as the best-fitting copula in this study, suggests that

469 $\hat{H}^2$ values greater than 7.8 correspond to precipitation events less than 0.6 mm, and $\hat{H}^2$ values

470 less than -0.3 correspond to precipitation events greater than 28.4 mm (Figure 7D). Conversely,

471 low frequencies are given to pairwise events when $\hat{H}^2$ and precipitation values are both low

472 ($\hat{H}^2 < $ -0.3 & precipitation < 0.6 mm) or high ($\hat{H}^2 > $ 7.8 & precipitation > 28.4 mm) (Figure

473 7D). In summary, the copula identifies and quantifies the tail-end relationship (as previously

474 highlighted by AghaKouchak et al. 2010) between $\hat{H}^2$ and precipitation that was not evident in

475 the simple correlation coefficient. An inverse, non-linear relationship between $\hat{H}^2$ and

476 precipitation was also suggested by the individual probability distributions of Figure 2.

477

478 **4.4. Daily winter precipitation forecasting**

479 **4.4.1. Precipitation estimations by ACCESS-R**

480 The daily ACCESS-R precipitation forecasts serve as our control forecast for the full two-

481 year (2014-2015) winter (May-October) period. When these precipitation forecasts were

482 evaluated against Snowy Hydro's high-elevation surface observations, the overall RMSE was

483 4.20 mm with a bias of 0.3 mm. On average ACCESS-R slightly overestimated the surface

484 observations. Looking at observed rain days only (0.25 mm day^{-1} threshold), the hit rate for

485 ACCESS-R was 88% with an RMSE of 6.2 mm day^{-1} and a bias of 0.42 mm day^{-1}. For no-

486 rain days, the false alarm rate was 20.7% with an RMSE of 0.58 mm day^{-1} and a bias of 0.19

487 mm day^{-1}.

488 These basic statistics can readily be broken down into the four clusters (Table 7). As

489 expected, the wet 'frontal' cluster, C1, has the highest percentage of rain days, the greatest

490 overall RMSE of 10.17 mm day^{-1} and bias of 0.76 mm day^{-1}. For rain days only, the hit rate

491 was 97%. Over the two-years of data (no-rain days), the false alarm rate was calculated to be

492 for C1. The relatively wet 'post-frontal' cluster, C2, shows the next highest overall percentage

493 of hits (69%) and RMSE (5.2 mm day^{-1}). The overall bias for C2 is 0.3 mm day^{-1}. Most notable

494   for this cluster is the high rate of false alarm (38%) when looking at no-rain days. ACCESS-R

495   produces precipitation too readily in these post-frontal conditions. For the dry clusters, C3 and

496   C4, the overall RMSE are small. They are less skilled on rain days (hit rates of 86 and 72%,

497   respectively) and relatively skilled on no-rain days (false alarm rates of 27 and 13%,

498   respectively).

499   More advanced metrics can readily be employed on these observations to assess the skill

500   of deterministic precipitation forecasts, following the World Meteorological Organization

501   Working Group on Numerical Experimentation (WWRP/WGNE 2008). For example, the

502   frequency bias score (FBS, the ratio of the frequency of forecast precipitation events to that of

503   observed; where 1 indicates a perfect score) was calculated to be 1.12, and 0.97, 1.05, 1.24,

504   1.16 for the overall time period and then broken down by cluster, respectively. An FBS score

505   greater than one suggests that the model generally tends to predict rain days more frequently

506   than they are observed. The absence of false alarm in C1 led to an FBS score of just under

507   unity, indicating the tendency to less frequently predict precipitation, however the opposite

508   occurred in the rest of the classes. The equitable threat score (ETS, the fraction of correctly

509   predicted of observed and/or forecast events that has a range of -1/3 to 1, where 0 indicates no

510   skill and 1 is a perfect score.) was calculated to be 0.49, and 0.73, 0.39, 0.41, 0.39 for the

511   overall time period and the four clusters, respectively. The ETS accounts for correct forecasts

512   due to chance when computing an index that combines the hit rate and the false alarm ratio.

513   Ebert (2001) finds an ETS of around 0.4 for the Poor Man's Ensemble precipitation predictions,

514   suggesting that the present system is especially skilful in identifying heavy-precipitation events.

515   The accuracy score (The fraction of "correct" forecasts) was also calculated to be 0.83, 0.97,

516   0.84, 0.79, 0.84 for the overall time period and the four clusters, respectively, indicating an

517   encouraging result, with the most accurate forecast in C1.

518

4.4.2. Model-1: Single regression model

The single regression model (Model 1) is based on only two predictors, a linear combination of the ACCESS-R precipitation forecast and QU (Table 8), determined by the stepwise approach and the BIC. The ACCESS-R forecast accounts for about 70% of the variance while QU contributed roughly 14%. Four goodness-of-fit criteria [RMSE, r^2 (the coefficient of determination), the hit rate, and bias (for all days)] are calculated to quantify the improvement in using a simple regression formula from the control ACCESS-R forecast precipitation (Table 9).

When limited to forecast precipitation days, the straight ACCESS-R forecast had an RMSE of 6 mm day^{-1}, a bias of 0.68 mm day^{-1} and a hit rate of 76% for the full two-year period (Results in Table 9 are different than those previously presented in Table 7 as the selection of rain day was changed from the surface observations to the ACCESS-R forecast to allow for an operational application). When the single regression model is applied, forecast precipitation had an RMSE of 5.6 mm day^{-1}, a bias of -0.15 mm day^{-1}, a hit rate of 78% and r^2 at 0.83. The single regression produced a 7% reduction in the RMSE. We can examine the forecast rain days by cluster, even when employing a single regression. The single regression model improves the RMSE in all four clusters, most strongly in C4. The bias is also reduced in each of the four clusters, most strongly in C4 and C1. The coefficient of determination remains largely unchanged by cluster. The single regression does not strongly improve one or more clusters at the expense of the remaining clusters. The improvement is largely across all clusters.

4.4.3. Model-2: Cluster-based regression model

The cluster-based regression (Model 2), produces an RMSE of 4.2 mm day^{-1}, a bias of -0.1 mm day^{-1}, an r^2 of 0.89 and a hit rate of 84% when computed over all days. The RMSE was

543 reduced by 30% and the bias was reduced by 7% in comparison to the control ACCESS-R

544 forecast precipitation.

545   When breaking this down into the individual clusters, large improvements are identified in

546 C1 (24% reduction in RMSE) and C4 (42% reduction in RMSE). Further r^2 increases most for

547 these two clusters. While the gains for cluster C2 were more modest (C2 has the simplest

548 regression fit), improvement is evident for all goodness of fit criteria. The cluster based

549 regressions also reduced the false alarm rate (as well as improving the hit rate) in all clusters,

550 but more strongly in the two wet ones.

551   Histograms of goodness-of-fit criteria for the cluster-based regression model for C1 (Model

552 2 C1) derived from cross-validation analysis are illustrated in Figure 8. Due to the presence of

553 skewness in histograms of coefficients and goodness-of-fit criteria (Figure 8), for all models,

554 median of the histograms is considered and reported to reduce the influence of outliers. Similar

555 histograms are obtained for other classes but not shown. It should be noted that the RMSE and

556 bias histograms are derived from the normalized values of estimations which are converted to

557 mm for the final comparisons between the models.

558

559 **5. Conclusion:**

560   A primary aim of this research has been to better understand the sensitivity of precipitation

561 over the Snowy Mountains of southeast Australia to the low-level stability (as measured by the

562 square of the non-dimensional mountain height, $\hat{H}^2$) and to understand the relationship

563 between the low-level stability and the synoptic meteorology, if any. A further aim has been to

564 exploit any uncovered relationship between the non-dimensional mountain height and

565 precipitation to improve forecasts of precipitation over these mountains for water management

566 purposes.

567   It has long been appreciated that orographic precipitation is sensitive to $\hat{H}^2$ with strong

568   stability (large $\hat{H}^2$) suppressing rainfall and, conversely, weak stability enhancing orographic

569   precipitation (e.g. Watson and Lane, 2014). An analysis of 21 years of wintertime data

570   confirmed this relationship for the Snowy Mountains. Average $\hat{H}^2$ was significantly greater for

571   no-rain days (14.5) than for rain days (3.9). A rain day was defined by a threshold of 0.25 mm

572   day^{-1}. A deeper analysis of these data found that the relationship was primarily driven by

573   extreme values with very large values of $\hat{H}^2$ (>7.8) being associated with suppressed rainfall

574   and very heavy rainfalls (>28 mm day^{-1}) being associated with low values of $\hat{H}^2$.

575   Previous research (D14) demonstrated that the precipitation over these mountains is also

576   sensitive to the large scale synoptic meteorology. Following this methodology, a K-means

577   clustering algorithm was applied to the precipitation using six synoptic predictors (GP, TW,

578   QU, QV, SH and TT). As before, four clusters were identified as the minimum number of

579   clusters necessary to distinguish the precipitation distribution between clusters. Examining

580   these more thoroughly with the use of ERA-I reanalysis data, the wet cluster (C1) was

581   associated with frontal passages. C2 was also a wet cluster, being associated with post-frontal

582   conditions. C4 was a dry cluster associated with suppressed (stable) conditions, and C3 was a

583   dry cluster constructed from the remaining observations. Distributions of $\hat{H}^2$ were also

584   distinguished by this clustering, suggesting that $\hat{H}^2$ was also strongly defined by the synoptic

585   meteorology.

586   When repeating the clustering for seven variables (the original six predictors plus $\hat{H}^2$), only

587   minor changes were observed for the two wet clusters, while changes were observed in the

588   number and composition of dry clusters, C3 and C4. A further investigation on the relationship

589   between the seven predictors and the observed precipitation showed that they are all

590   statistically correlated, justifying their application in forecasting orographic precipitation.

591 Higher values in rank correlations of the stability indicators (more obviously for $\hat{H}^2$) suggested

592 a non-linear relationship rather than linear relationship.

593 D14 noted that over the Snowy Mountains a NWP model demonstrated more skill at

594 predicting the synoptic meteorology than the precipitation. Thus, model output statistics (MOS)

595 of the synoptic variables was used to improve precipitation forecasts. Two different regression

596 models were developed with the aim of improving the precipitation forecasts of the ACCESS-

597 R model. Specifically, the goal was to reduce the RMSE and bias. First a single regression

598 model was developed and applied to two-years (2014-2015 wintertime) of ACCESS-R

599 precipitation forecasts. This led to a 7% reduction in the RMSE and a 78% reduction in the

600 bias. Then, a cluster-based regression was applied leading to a 30% reduction in the RMSE and

601 an 85% reduction in the bias.

602 The stepwise-based regression method (Curtis and Ghosh 2011) employed initially seeks a

603 leading predictor that is able to convey a large portion of the dependent variable information

604 (i.e. the ACCESS_R precipitation forecasts). Following on, the regression methodology tries

605 to select another leading predictor to further improve the accuracy of forecasts. While

606 additional predictors will improve accuracy, they are only added if they avoid redundancy,

607 collinearity and complexity. It is important to note that all of the tested indicators have already

608 been utilized as input variables to the clustering algorithm. Having TT as a leading predictor

609 in C1 suggests that the model systematic error may be mostly associated with the variation of

610 large-scale stability. Following this logic, the model precipitation overestimation in C4 may be

611 rooted in misrepresentation of moisture flux.

612 A potential extension of this work could be to consider the application of statistical

613 adjustments for forecasts at longer lead times. The ACCESS-VT model only runs for 36 hours,

614 preventing such testing on the immediate observations and simulations. As the accuracy of the

24

615 ACCESS system continues to improve, the main value of such statistical analysis may be in

616 the identification of the source of systematic errors in the system.

617

618 **Acknowledgments:**

623

624 **References:**

625 AghaKouchak, A., Ciach, G., Habib, E. 2010: Estimation of tail dependence coefficient in
626   rainfall accumulation fields. *Adv Water Resour.* 33 (9): 1142-1149.

627 Bureau of Meteorology (BoM) 2017: East Coast Lows, http://www.bom.gov.au/nsw/
628   sevwx/facts/ecl.shtml. Last Access: 20-March-2017.

629 Chubb, T.H., S.T. Siems, and M.J. Manton, 2011: On the decline of wintertime precipitation
630   in the Snowy Mountains of southeastern Australia. *J. Hydrometeor.*, 12, 1483–1497,
631   DOI:10.1175/JHM-D-10-05021.1.

632 ——, A. E. Morrison, S. Caine, S. T. Siems, and M. J. Manton, 2012: Case studies of
633   orographic precipitation in the Brindabella Ranges: Model evaluation and prospects for
634   cloud seeding. *Aust. Meteor. Oceanogr. J.*, 62, 305–321.

635 ——, M.J. Manton, S.T. Siems, A.D. Peace, and S.P. Bilish, 2015: Estimation of wind-induced
636   losses from a precipitation gauge network in the Australian Snowy Mountains. *J.
637   Hydrometeor.*, 16, 2619-2638

638 ——, M.J. Manton, S.T. Siems, and A.D. Peace. 2016. Evaluation of the AWAP daily
639   precipitation spatial analysis with an independent gauge network in the Snowy Mountains.
640   J. Southern Hemisphere Earth System Science. 66: 55-67

641 Colle, B. A., 2004: Sensitivity of orographic precipitation to changing ambient conditions and
642   terrain geometries: An idealized modeling perspective. *J. Atmos. Sci.*, 61, 588–606.

643 Curtis, S.M. and S.K. Ghosh, 2011: A Bayesian Approach to Multicollinearity and the
644   Simultaneous Selection and Clustering of Predictors in Linear Regression, *Journal of
645   Statistical Theory and Practice*, 5:4, 715-735.

646 Dai J, Manton MJ, Siems ST. 2014. Estimation of daily winter precipitation in the Snowy
647   Mountains of southern Australia. *J. Hydrometeor*. 14: 909-920.

648 Davies, T., M.J.P. Cullen, A.J. Malcolm, M.H. Mawson, A. Staniforth, A.A. White, and N.
649   Wood, 2005: A new dynamical core for the Met Office's global and regional modelling of
650   the atmosphere. *Q. J. R. Meteorol. Soc.* 131: 429–451, doi: 10.1256/qj.04.1016.

651 Dee, D. P., and co-authors, 2011: The ERA-Interim reanalysis: Configuration and performance
652   of the data assimilation system. *Quart. J. Roy. Meteor. Soc.*, 137, 553–597, DOI:10.1002/
653   qj.828.

654 Drouet-Mari, D., Kotz. S. 2001: Correlation and Dependence. London: Imperial College Press.

655 Durran, D., and J. Klemp, 1982: On the effects of moisture on the Brunt-Vaisala frequency. *J.
656   Atmos. Sci.,* 39, 2152–2158.

657 Ebert, E. E., 2001: Ability of a poor man's ensemble to predict the probability and distribution
658   of precipitation. *Mon. Wea. Rev.*, 129, 2461–2480, doi:10.1175/1520 0493(2001)129,2461:
659   AOAPMS.2.0.CO;2; Corrigendum, 130, 1661–1663.

660 Fiddes, S.L., A.B. Pezza, and V. Barras, 2015: Synoptic climatology of extreme precipitation
661   in alpine Australia. *Int. J. Climatol*. 35: 172–188. DOI: 10.1002/joc.3970.

662 Frank, M.J. 1979: On the Simultaneous Associativity of F(x,y) and x+y−F(x, y). Aequationes
663   Mathematicae, 19, 194–226.

664 Gallant, A.J.E., A.S. Kiem, D.C. Verdon-Kidd, R.C. Stone, and D.J. Karoly, 2012:
665   Understanding hydroclimate processes in the Murray-Darling Basin for natural resources
666   management. *Hydrol. Earth Syst. Sci.*, 16, 2049–2068, doi:10.5194/hess-16-2049-2012.

667 Genest, C., Plante, J.F. 2003: On Blest's measure of rank correlation. *The Canadian Journal
668   of Statistics,* 31:1–18.

669 Glahn, H.R., D. A. Lowry, 1972: The use use of Model Output Statistics (MOS) in objective
670   weather forecasting. *J. Appl. Meteor., 11, 1203-1211.*

671 Hartigan, J., and M. Wong, 1979: A K-means clustering algorithm. *J. Roy. Stat. Soc.*, 28C,
672   100–108, doi:10.2307/2346830.

673 Henry, N. L., 2000: A static stability index for low-topped convection. *Wea. Forecasting*, 15,
674   246–254, DOI:10.1175/1520-0434(2000)015,0246:ASSIFL.2.0.CO.2.

675 Houze, R.A. 2012: Orographic effects on precipitating clouds. *Rev. Geophys*. 50.

676 Hughes, M., A. Hall, and R.G. Fovell, 2009: Blocking in areas of complex topography and its

677 influence on rainfall distribution. *Journal of the Atmospheric Sciences*. DOI:

678 10.1175/2008jas2689.1.

679 Landvogt, P., J. Bye, and T. Lane, 2008: An investigation of recent orographic precipitation

680 events in north-east Victoria. Aust. Meteor. Mag., 57, 235–247.

681 Liebscher, G. 2012. A Universal Selection Method in Linear Regression Models. *Open Journal*

682 *of Statistics*, 153-162.

683 Madadgar, S., and H. Moradkhani, 2014: Improved Bayesian Multi-Modeling: Integration of

684 Copulas and Bayesian Model Averaging. *Water Resour. Res.*, 50, 9586–9603.

685 Miglietta, M. M., and A. Buzzi, 2001: A numerical study of moist stratified flows over

686 isolated topography. *Tellus*, 53A, 481–499.

687 Morrison, A. E., S. T. Siems, and M. J. Manton, 2013: On a natural environment for glaciogenic

688 cloud seeding. *J. Appl. Meteor. Climatol.*, 52, 1097–1104, doi:10.1175/JAMC-D-12-0108.1.

689 Nicoloutsopoulos, D. 2005: Parametric and Bayesian non-parametric estimation of copulas.

690 PhD thesis, University College London.

691 Nguyen, H., A. Protat, V. Kumar, S. Rauniyar, M. Whimpey, and L. Rikus, 2015: A regional

692 forecast model evaluation of statistical rainfall properties using the CPOL radar

693 observations in different precipitation regimes over the Darwin, Australia. *Q. J. R. Meteorol.*

694 *Soc*. 141: 2337–2349.

695 Osburn, L., T. Chubb, S. Siems, M. Manton, and A.D. Peace, 2016: Observations of

696 Supercooled Liquid Water in Wintertime Alpine Storms in South Eastern Australia.

697 *Atmospheric Research*, 169, 345–356.

698 Pan, M., Yuan, X., and Wood, E. F. 2013: A probabilistic view on drought recovery, *Geophys.*

699 *Res. Lett.*, 40, 3637–3642.

700 Panziera, L. 2010: Orogeraphic forcing, the key for heuristic nowcasting of rainfall in the Alps.

701 PhD dissertation, ETH Zurich.

702 Patton, A.J. 2012. A review of Copula models for economic time series. *Journal of Multivariate*

703 *Analysis*, V110: 4-18. DOI: 10.1016/j.jmva.2012.02.021.

704 Pierrehumbert, R. T., and B. Wyman, 1985: Upstream effect of mesoscale mountains. *J. Atmos.*

705 *Sci.*, 41, 977-1003.

706 Puri, K., and co-authors, 2013: Implementation of the initial ACCESS numerical weather

707 prediction system, *Aus. Meteorol. Oceanogr. J.* 63, 265-284.

708   Pook, M.J., P.C. McIntosh, and G.A. Meyers, 2006: The synoptic decomposition of cool-

709   season rainfall in the southeastern Australian cropping region. *J. App. Meteor. Climatol.*, 45,

710   1156-1170, doi:10.1175/JAM2394.1.

711   Miao, Q. and B. Geerts, 2013: Airborne measurements of the impact of ground-based

712   glaciogenic cloud seeding on orographic precipitation. *Adv. Atmos. Sci.* 30: 1025.

713   doi:10.1007/s00376-012-2128-2.

714   Reinecke, P.A., and D.R. Durran, 2008: Estimating topographic Blocking using a Froude

715   Number when the static stability is non-uniform. *J. of the Atmospheric Sciences*, 65, 1035-

716   1048, DOI:10.1175/2007JAS2100.1.

717   Risbey, J.S., M.J. Pook, P.C. McIntosh, M.C. Wheeler, and H.H. Hendon, 2009: On the remote

718   drivers of rainfall variability in Australia, *Monthly Weather Review*, DOI:

719   10.1175/2009MWR2861.1.

720   Saji, N., B.Goswami, P.Vinayachandran, and T. Yamagata, 1999: A dipole mode in the tropical

721   Indian Ocean. *Nature*, 401, 360–363.

722   Schweizer, B., and E.F. Wolff, 1981: On nonparametric measures of dependence for random

723   variables. *The Annals of Statistics*, Vol. 9, No. 4, 879-885.

724   Shrestha, D.L., D.E. Robertson, Q.J. Wang, T.C. Pagano, and H.A.P. Hapuarachchi, 2013:

725   Evaluation of numerical weather prediction model precipitation forecasts for short-term

726   streamflow forecasting purpose. *Hydrol. Earth Syst. Sci.*, 17, 1913–1931.

727   Sklar, A. 1959: Fonctions de repartition `a n dimensions et leurs marges. Publications de

728   l'Institut de Statistique de l'Universit´e de Paris 8:229–231.

729   Smith, R. B., 1989: Hydrostatic airflow over mountains. *Advances in Geophysics*, Vol. 31,

730   Academic Press, 1–41.

731   Theobald, A., H. McGowan, J. Speirs, and N. Callow, 2015: A synoptic classification of

732   Inflow-Generating precipitation in the Snowy Mountain, Australia. *Journal of Applied*

733   *Meteorology and Climatology*, 54, 1035-1047, DOI: 10.1175/JAMC-D-14-0278.1.

734   Timbal, B., 2009: The continuing decline in south-east Australian rainfall: Update to May

735   2009. *CAWCR Res*. Lett., 2, 4–11.

736   Thomson, D., Cited 2007: A brief introduction to the annular modes and annular research.

737   [Available online at http://www.atmos.colostate.edu/ao/.].

738   Vernieuwe, H., Vandenberghe, S., De Baets, B., and Verhoest, N. E. C. 2015: A continuous

739   rainfall model based on vine copulas, *Hydrol. Earth Syst. Sci.*, 19, 2685-2699,

740   doi:10.5194/hess-19-2685-2015.

741 Wang, G., and H. Hendon, 2007: Sensitivity of Australian rainfall to inter–El Nino variations.

742 *J. Climate*, 20, 4211–4226.

743 Wang, Z., Belusic, D., Huang, Y., Siems, S.T., and M.J. Manton, 2016: Understanding

744 Orographic Effects on Surface Observations at Macquarie Island. Journal of Applied

745 Meteorology and Climatology, DOI: 10.1175/JAMC-D-15-0305.1.

746 Watson, C.D. and T.P. Lane, 2014: Further sensitivities of orographic precipitation to terrain

747 geometry in idealized simulations. J. Atmos. Sci., 71, 3068–3089, doi:10.1175/JAS-D-13-

748 0318.1.

749 Wilson, L., M. J. Manton, and S. T. Siems, 2013: Relationship between rainfall and weather

750 regimes in south-eastern Queensland, Australia. *Int. J. Climatol.*, 33, 979–991, doi:10.1002/

751 joc.3484.

752 WWRP/WGNE. 2008. Recommendations for the verification and inter-comparison of QPFs

753 and PQPFs from operational NWP models. 37 pp., Geneva, Switzerland.

754

755

756

757

758

759

760

761

762

763

764

765

766

767

768

769

770

771

772

773

Figure captions:

Figure 1. a) Map of the Snowy Mountains analysis region (red box) in southeastern Australia showing the closest upper-wind site of the BoM to the Snowy Mountains (Wagga Wagga). b) Location of the seven alpine rain gauges used in this study (enlarged red box).

Figure 2. Probability distribution of daily winter rainfall (left panel) and $\hat{H}^2$ (right panel) for next 24 hours after sounding measurements over the period 1995-2015 based on six large-scale synoptic indicators.

Figure 3. a-d) Distribution of $\hat{H}^2$ for each cluster, e) stacked histograms of $\hat{H}^2$ variable for different clusters, f) the $\hat{H}^2$ distribution for No-Rain days and Rain days. ($\hat{H}^2$ >25, occurring ~7% of the time and mostly in C4 are not shown). Note the different axes in (e and f) compared to (a-d)

Figure 4. Composite charts of MSLP in *hPa* (Top) and TW in $hPa.s^2.m^{-1}$ (bottom), showing total moisture up to 250-*hPa*, for the four classes. Era-Interim data (00UTC, May-October, 1995-2015) at a spatial resolution of $0.75° \times 0.75°$ used to construct composite maps of only the top 25% of days of each cluster with the shortest Euclidean distance to the cluster centre. The corresponding maximum and minimum values of the examined variables are shown on top of the individual panels.

Figure 5. As in Figure 4, but showing QV and QU (westerly and southerly moisture flux up to 250-*hPa*) for the four classes. Color-filled contours shows the magnitude of the moisture fluxes ($\sqrt{QU^2 + QV^2}$) in *Kg s⁻¹ m⁻¹* and arrows of the same length represent the moisture flux direction.

Figure 6. As in Figure 4, but showing total totals index (TT) in ℃ and root-mean-square wind shear between 850 and 500 *hPa* (SH) in $1/s$.

Figure 7. A) Histogram and scatter plot of precipitation and $\hat{H}^2$, B & C) the marginal CDF distributions of precipitation and $\hat{H}^2$. D) Joint frequency using Frank PDF copula. All the graphs are based on the data from 1995-2015 (for rainy days).

807   Figure 8. Histograms of goodness-of-fit criteria (RMSE, r^2, and Bias) based on normalized

808   values for Model-2_C1 derived from cross-validations with 10000 simulations. The median of

809   each panel is taken to represent the average values in Table 8.

810

811

812

813

814

815

816

817

Table 1. Properties of precipitation gauges sites at high altitudes in the Snowy Mountains. The mean winter precipitation values are calculated over the period 1995-2015.

Site	Start Year	Longitude (º)	Latitude (º)	Elevation (m)	Mean winter Precipitation (mm)
Tooma Dam	1992	148.28	-36.05	1221	1156.96
Geehi Dam	1992	148.31	-36.30	1175	1054.92
Jagungal	1990	148.39	-36.14	1659	1104.37
The Kerries	1995	148.38	-36.26	1740	1027.27
Guthega Dam	1992	148.37	-36.38	1175	881.84
Guthega Power Station	1994	148.41	-36.35	1320	963.30
Cabramurra	1955	148.38	-35.94	1482	857.69

820

821

822

823

824

825

826

827

828

829

830

831

832

833

834

835

836

837

838

839

840

841 Table 2. Summary of six synoptic indicators used to represent large-scale environment.

Variables	Abbreviation	Formula	Unit
Surface pressure at Wagga Wagga	GP	Non-Applicable	hPa
Southerly moisture flux up to 250 hPa	QV	$\frac{1}{g}\int qVdp$	$Kg\ s^{-1}\ m^{-1}$
Westerly moisture flux up to 250 hPa	QU	$\frac{1}{g}\int qUdp$	$Kg\ s^{-1}\ m^{-1}$
Total moisture up to 250 hPa	TW	$\frac{1}{g}\int qdp$	$hPa.s^2.m^{-1}$
Root-mean-square wind shear between 850 and 500 hPa	SH	$\sqrt{(\frac{\Delta U}{\Delta z})^2 + (\frac{\Delta V}{\Delta z})^2}$	s^{-1}
Total totals index	TT	$T(850) - 2T(500) + T_d(850)$	^oC

842

843

844

845

846

847

848

849

850

851

852

853

854

855

856

857

858

859

860

861

862 Table 3. Main statistical characteristics of daily winter precipitation in mm for rainy days (>0.25mm).

863 Numbers shown in the brackets are the ACCESS-R results for a 2-yr period.

	Observations (1995-2015)						Observations (ACCESS-R) (2014-15)	
Month	Rainy days' Frequency	Average Monthly (mm)	Mean Intensity (mm/day)	1st Quartile	2nd Quartile	3rd Quartile	Rainy days' Frequency	Mean Intensity
May	41%	122.5	9.5	6.7	9.8	12.8	51% (55%)	8.8 (8.4)
June	56%	171.5	10.6	5.7	10.6	14.2	50% (50%)	10.8 (12.0)
July	63%	179.6	9.7	8.3	9.5	11.7	58% (64%)	8.8 (9.7)
August	60%	193.1	10.9	9.0	10.6	13.4	55% (52%)	6.3 (5.4)
September	53%	192.1	11.6	10.0	11.7	13.0	35% (49%)	6.9 (7.4)
October	44%	143.3	10.0	6.4	9.1	13.1	23% (40%)	8.2 (10.1)
May-Oct	52%	166.7	10.4	7.7	10.2	13	45% (51%)	8.3 (8.8)

864

865

866

867

868

869

870

872

Table 4. Main statistical characteristics of daily winter rainfall and $\hat{H}^2$ across synoptic clusters.

Clusters	Frequency			Mean	1st Quartile		2nd Quartile		3rd Quartile	
	All days	**Rainy days**	**Unblocked* All days (rainy days)**	**Rainfall (rainy days) mm**	**Rainfall mm**	$\hat{H}^2$	**Rainfall mm**	$\hat{H}^2$	**Rainfall mm**	$\hat{H}^2$
C1	9.9%	93%	63% (66%)	22.94	5.74	0.05	17.48	0.7	29.04	1.7
C2	22.2%	78%	48% (53%)	10.83	0.63	0.03	4.54	1.11	12.87	3.01
C3	39.2%	52%	20% (30%)	6.12	0	1.35	0.32	3.33	8.7	3.66
C4	28.6%	22%	5% (12%)	3.32	0	4.59	0.03	11.1	0.17	27.88

873 *Unblocked cases: days with $\hat{H}^2 < 1$.

874

875

876

877

878

879

880

881

882

883

885   Table 5. Cross-correlation coefficients between seven synoptic indicators.

	GP	SH	TT	TW	QV	QU	$\hat{H}^2$
GP		**-0.283**	**-0.361**	**-0.379**	**0.223**	**-0.530**	**0.338**
SH			**-0.136**	-0.030	-0.019	**0.334**	**-0.154**
TT				**0.516**	-0224	**0.149**	**-0.269**
TW					**-0.554**	**0.388**	**-0.237**
QV						**-0.297**	**0.155**
QU							**-0.249**
$\hat{H}^2$							

886   *Bold numbers are significant correlation at significant level of 1%.

887

888

889

890

891

892

893

894

895

896

897

898

899

900

901

902

903

904

905

906

907

908

909

910

911

912 Table 6. Linear and Rank correlation coefficients between seven synoptic indicators and
913 observed precipitation over the period of 1995-2015 (Classification results based on 7-variable
914 clustering).

		GP	SH	TT	TW	QV	QU	$\hat{H}^2$
C1	Linear	**-.206**	.018	-.039	**.176**	**-.482**	**.194**	**-.198**
	Rank	**-.261**	.019	.010	.063	**-.460**	**.143**	**-.296**
C2	Linear	**-.370**	.032	**.219**	**.197**	**-.181**	**.276**	**-.203**
	Rank	**-.400**	-.012	**.311**	**.166**	**-.161**	**.308**	**-.355**
C3	Linear	**-.288**	.002	.052	**.119**	**-.137**	**.144**	**-.180**
	Rank	**-.360**	.010	**.210**	**.124**	.002	**.218**	**-.344**
C4	Linear	**-.199**	**.114**	-.061	.041	**-.153**	**.194**	**-.098**
	Rank	**-.150**	**.151**	-.019	**-.073**	**.071**	**.161**	**-.215**
No Class	Linear	**-.464**	**.163**	**.232**	**.428**	**-.509**	**.465**	**-.237**
	Rank	**-.555**	**.186**	**.367**	**.376**	**-.231**	**.469**	**-.533**

915 *Bold numbers are significant correlation at significant level of 5%. No Class: no classification process
916 has been implemented.

917

37

918

919 Table 7. Performance of ACCESS-R precipitation estimation of observed precipitations over the period of 2014-15 with a value of 0.25 mm for
920 the rain-day threshold. (Hit, Miss, False Alarm and Correct/Negative values are in percentage)

Synoptic classes (No. of days)	All days						rain days only			No-rain days only		
	Hit	Miss	False-alarm	*Cor/Neg	RMSE (mm)	Bias (mm)	Hit rate	RMSE (mm)	Bias (mm)	False-alarm rate	RMSE (mm)	Bias (mm)
C1 (34)	88	3	0	9	10.2	0.76	97	10.7	0.83	0	0.03	-0.01
C2 (51)	69	6	10	16	5.2	0.3	92	6.0	0.15	38	1.50	0.73
C3 (141)	36	6	16	43	2.1	0.1	86	3.2	-0.04	27	0.41	0.2
C4 (110)	16	6	10	67	2.0	0.4	72	4.1	1.4	13	0.44	0.10
All days**(336)	40	6	11	43	4.2	0.3	88	6.2	0.42	21	0.58	0.19

921   *Cor/Neg: Correct/Negative: model correctly detects no rain days

922   ** All days: all days without implementing the classification.

923

924

925

926

927

928

929

930

931

932

933

934   Table 8. Leading predictors in regression equations for different models.

Model		Leading Predictors using stepwise algorithm coupled with BIC criteria on 8 indicators	Regression equation
1		QU, Prec_Acc	Y = Int. +αQU+βPrec_Acc+γQU×Prec_Acc
2	C1	TT, Prec_Acc	Y = Int. -αTT+βPrec_Acc+γTT×Prec_Acc
	C2	Prec_Acc	Y = Intercept +αPrec_Acc
	C3	QU, Prec_Acc	Y =Int.+αQU+β Prec_Acc+γQU×Prec_Acc
	C4	QV, Prec_Acc	Y = Int. -αQV+βPrec_Acc+γQV×Prec_Acc

935   Int.: Intercept

936

937

938

939

940

941

942

943

944

945

946

947

948

949

950

951

952

953

954

955

956

957

958

959

960

961

Table 9. Goodness-of-fit criteria for different models for estimating daily winter precipitations over 2014-15 based on ACCESS-R rainy days
(results are only for the test groups).

Classes	Models	Goodness-of-fit criteria				Improvement of model 1 and 2 in compare to ACCESS forecast for each criterion (%)			
		RMSE (mm)	r^2	BIAS (mm)	Hit rate	RMSE	r^2	BIAS	Hit
	ACCESS	6.0	0.83	0.68	76		NA		
Overall	1	5.6	0.83	-0.15	78	6.7	0.0	77.9	3.1
	2	4.2	0.89	-0.10	84	30.1	7.2	85.3	10.8
	ACCESS	10.8	0.67	1.10	90		NA		
C1	1	10.3	0.77	-1.30	93	4.0	14.9	-18.2	3.7
	2	8.2	0.81	-0.60	100	23.5	20.9	45.5	11.1
	ACCESS	5.9	0.82	0.48	90		NA		
C2	1	5.8	0.84	-0.34	93	2.2	2.4	29.2	2.8
	2	5.7	0.88	-0.19	100	3.9	7.3	60.4	11.1
	ACCESS	3.0	0.89	0.23	67		NA		
C3	1	2.7	0.90	-0.17	68	7.4	1.1	26.1	2.0
	2	2.6	0.91	-0.04	70	13.5	2.2	82.6	4.1
	ACCESS	3.9	0.62	1.70	62		NA		
C4	1	3.4	0.62	1.40	66	12.9	0.0	17.6	5.6
	2	2.3	0.69	-0.21	79	42.0	11.3	87.6	27.8
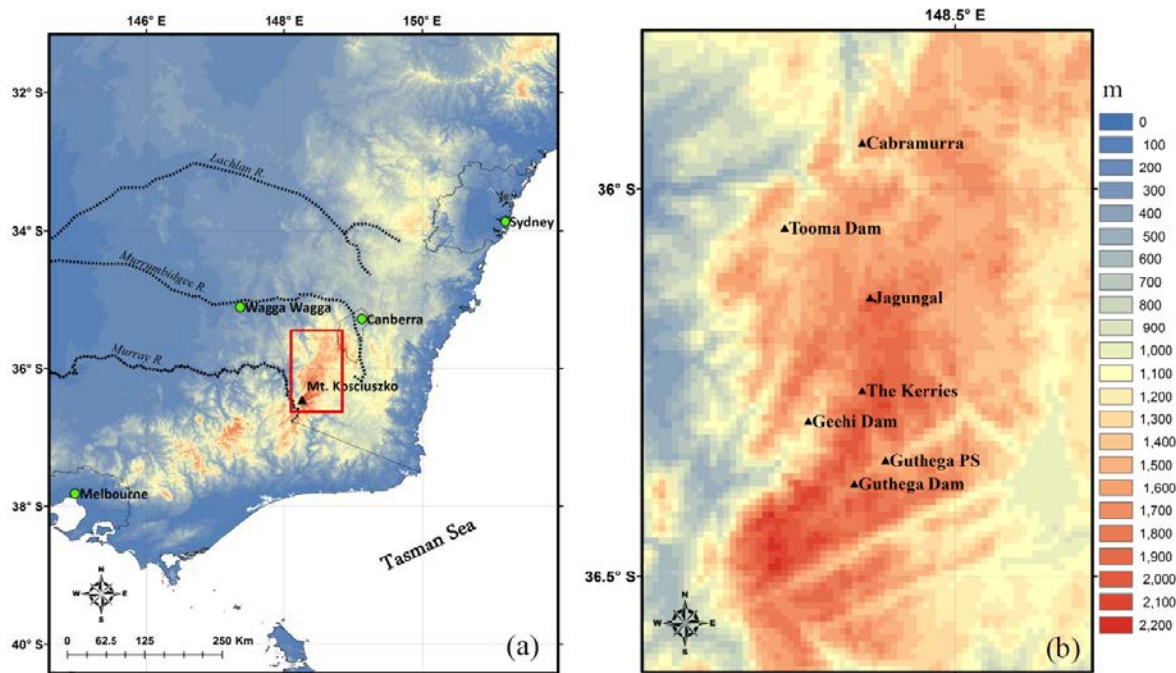
964 *NA: Not Applicable

Figure 1. a) Map of the Snowy Mountains analysis region (red box) in southeastern Australia showing the closest upper-wind site of the BoM to the Snowy Mountains (Wagga Wagga). b) Location of the seven alpine rain gauges used in this study (enlarged red box).

984
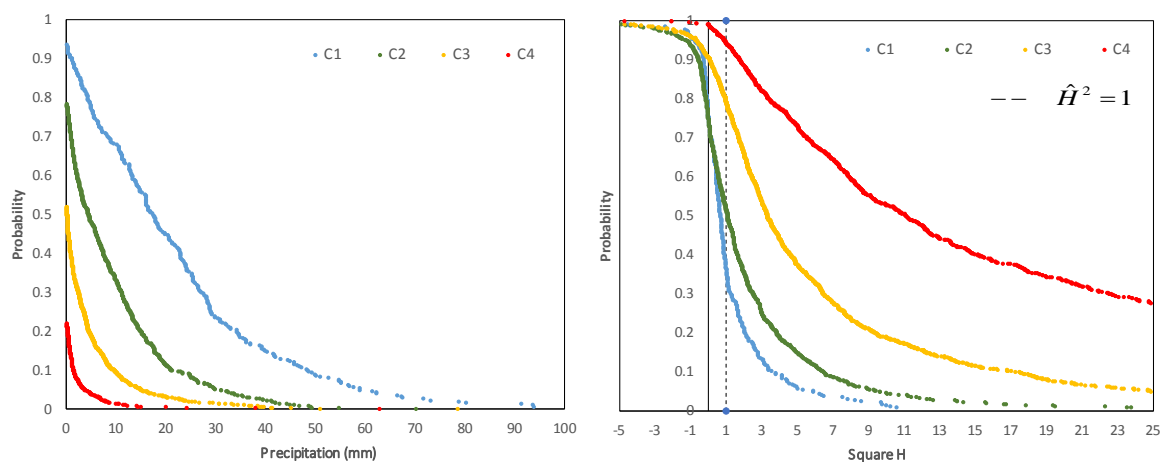
985

986 Figure 2. Probability distribution of daily winter rainfall (left panel) and $\hat{H}^2$ (right panel) for
987 next 24 hours after sounding measurements over the period 1995-2015 based on six large-scale
988 synoptic indicators.

989

990

991

992

993

994

995

996

997

998

999

1000

1001

1002

1003

1004

1005

1006

1007

1008

1009

1010

1011 Figure 3. a-d) Distribution of $\hat{H}^2$ for each cluster, e) stacked histograms of $\hat{H}^2$ variable for

1012 different clusters, f) the $\hat{H}^2$ distribution for No-Rain days and Rain days. ($\hat{H}^2 > 25$, occurring

1013 ~7% of the time and mostly in C4 are not shown). Note the different axes in (e and f) compared

1014 to (a-d)

1015

1016
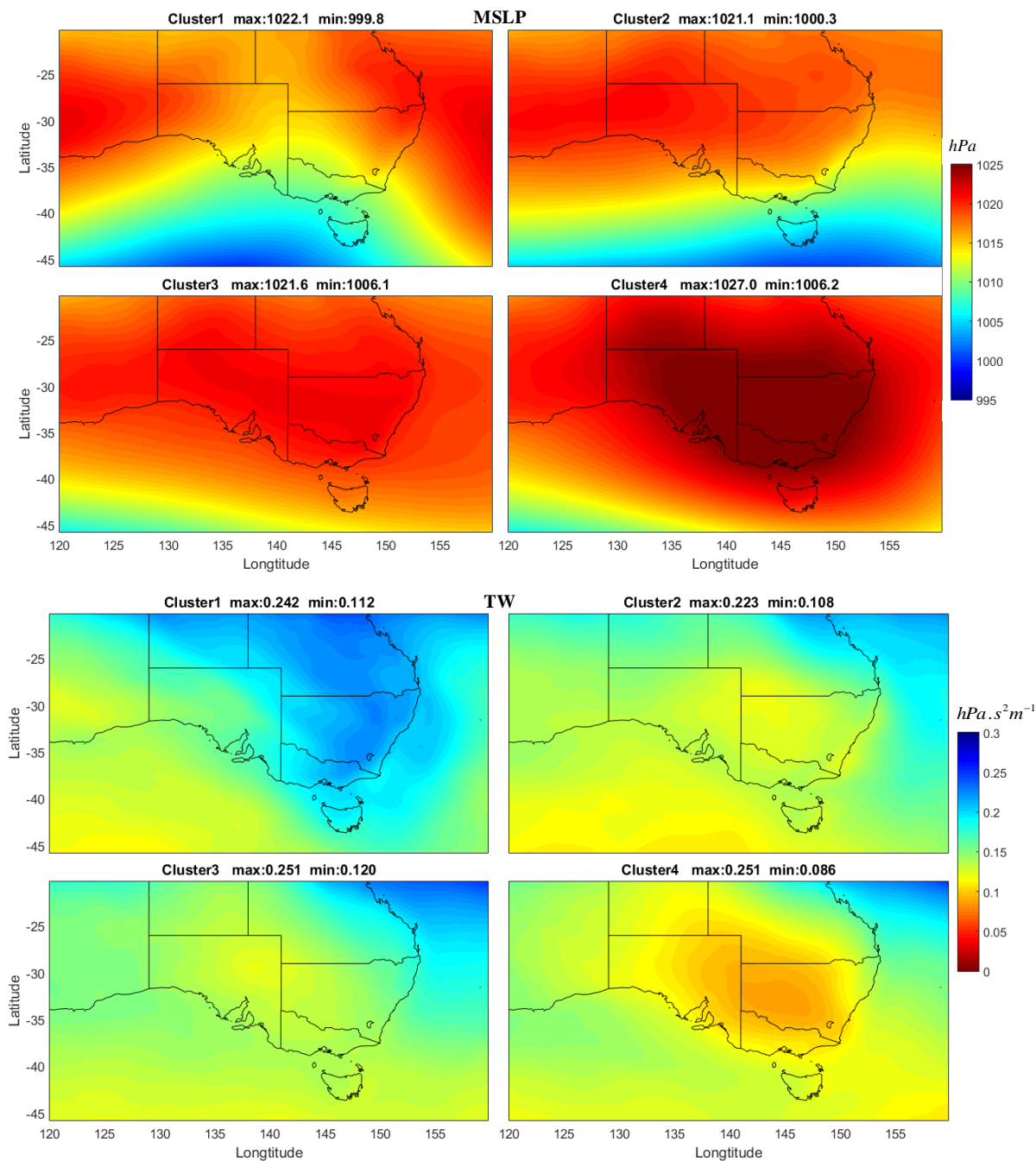
1017

Figure 4. Composite charts of MSLP in *hPa* (Top) and TW in $hPa.s^2/m$ (bottom), showing total moisture up to 250-*hPa*, for the four classes. Era-Interim data (00UTC, May-October, 1995-2015) at a spatial resolution of 0.75° × 0.75° used to construct composite maps of only the top 25% of days of each cluster with the shortest Euclidean distance to the cluster centre. The corresponding maximum and minimum values of the examined variables are shown on top of the individual panels.
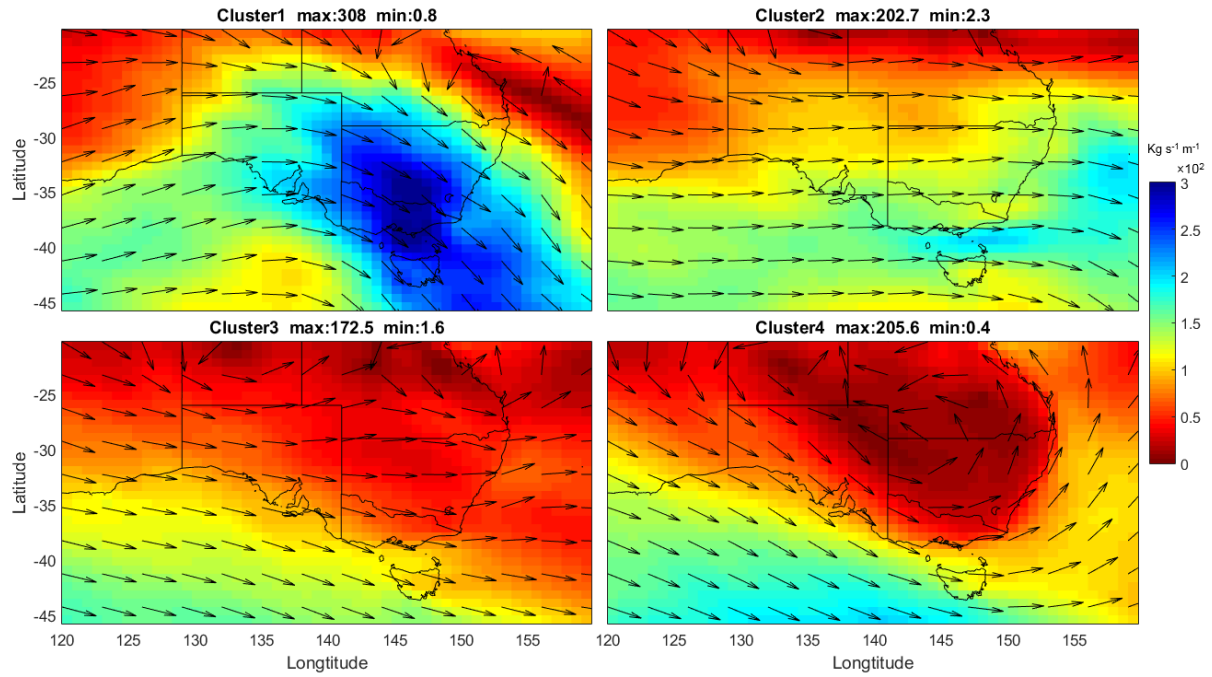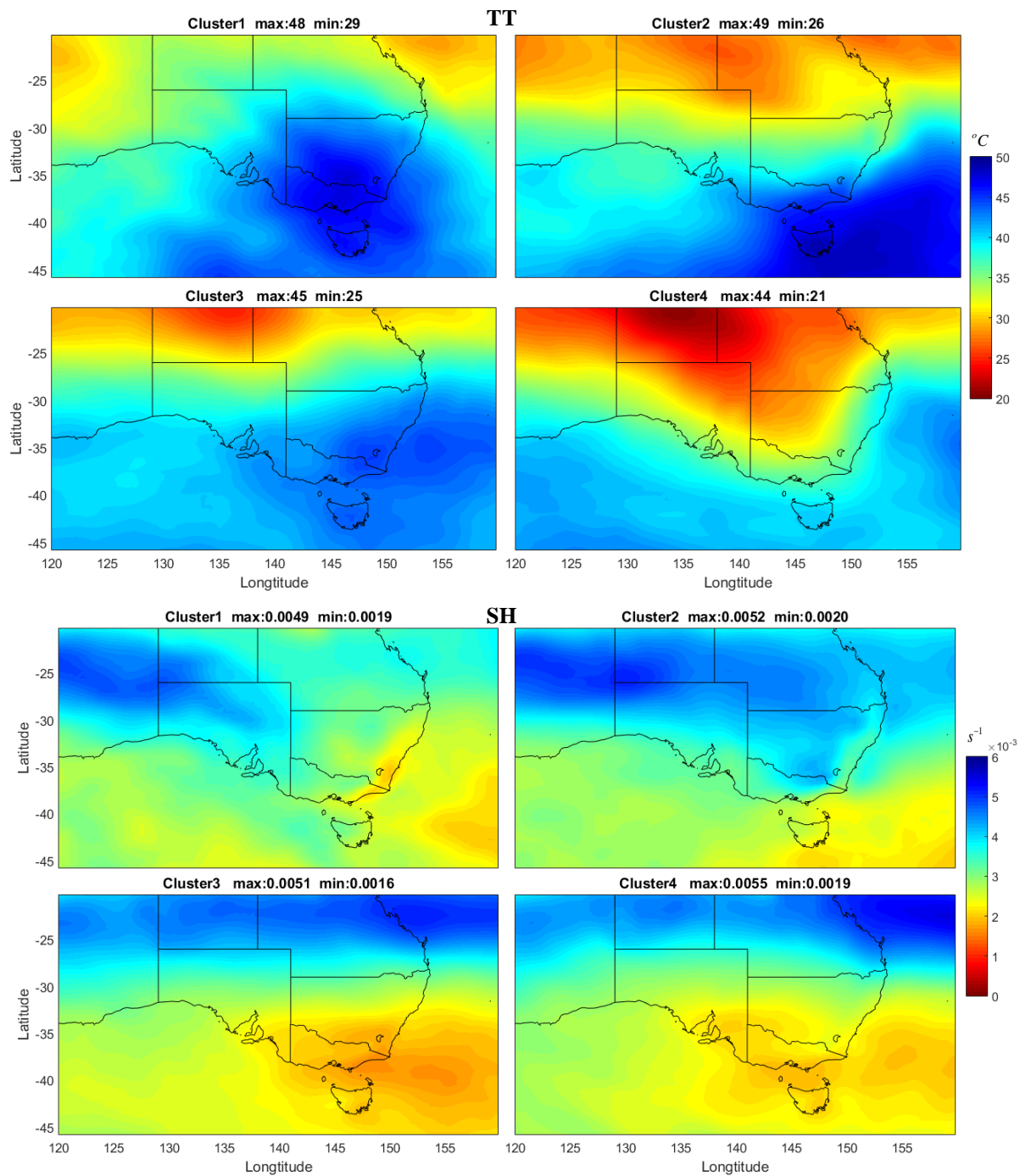
1024

1025

Figure 5. As in Figure 4, but showing QV and QU (westerly and southerly moisture flux up to 250-*hPa*) for the four classes. Color-filled contours shows the magnitude of the moisture fluxes ($\sqrt{QU^2 + QV^2}$) in *Kg s⁻¹ m⁻¹* and arrows of the same length represent the moisture flux direction.
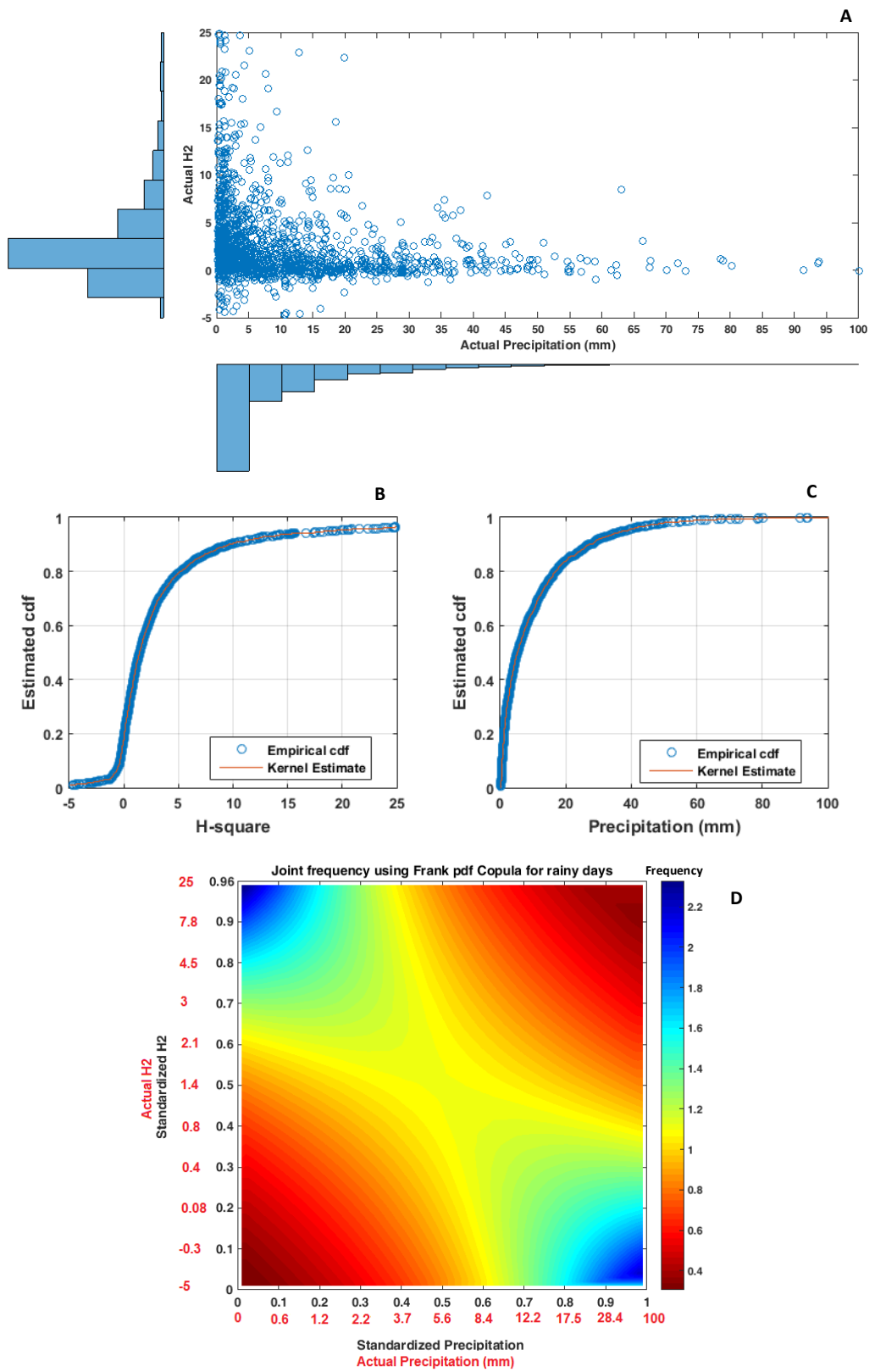
1049

1050

Figure 6. As in Figure 4, but showing total totals index (TT) in °C and root-mean-square wind

shear between 850 and 500 hPa (SH) in $1/s$.

1053

1054

1055

1056

Figure 7. A) Histogram and scatter plot of precipitation and $\hat{H}^2$, B & C) the marginal CDF distributions of precipitation and $\hat{H}^2$. D) Joint frequency using Frank PDF copula. All the graphs are based on the data from 1995-2015 (for rainy days).
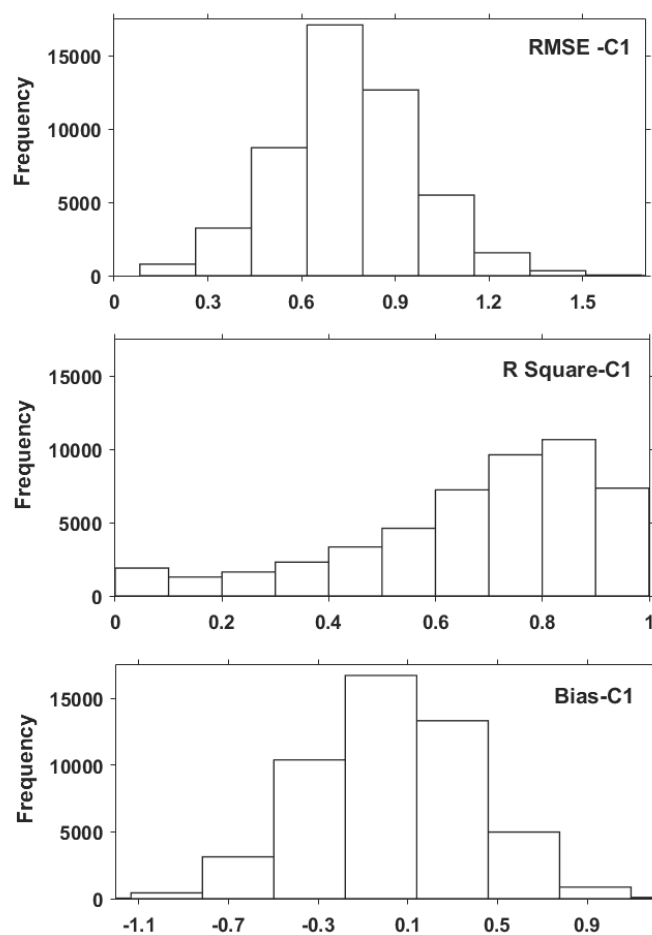
1062

1063 Figure 8. Histograms of goodness-of-fit criteria (RMSE, r^2, and Bias) based on normalized

1064 values for Model-2_C1 derived from cross-validations with 10000 simulations. The median of

1065 each panel is taken to represent the average values in Table 8.